Methane Aqueous Fluids in Montmorillonite Clay Interlayer under Near-Surface Geological Conditions: A Grand Canonical Monte Carlo and Molecular Dynamics Simulation Study

ARTICLE *in* THE JOURNAL OF PHYSICAL CHEMISTRY B · AUGUST 2014

Impact Factor: 3.3 · DOI: 10.1021/jp507884w · Source: PubMed

2 AUTHORS:

Qi Rao
George Washington University
6 PUBLICATIONS **29** CITATIONS
SEE PROFILE

Yongsheng Leng
George Washington University
56 PUBLICATIONS **767** CITATIONS
SEE PROFILE

THE JOURNAL OF PHYSICAL CHEMISTRY B

Article

pubs.acs.org/JPCB

Methane Aqueous Fluids in Montmorillonite Clay Interlayer under Near-Surface Geological Conditions: A Grand Canonical Monte Carlo and Molecular Dynamics Simulation Study

Qi Rao and Yongsheng Leng*

Department of Mechanical and Aerospace Engineering, The George Washington University, Washington, D.C. 20052, United States

Supporting Information

ABSTRACT: The grand-canonical Monte Carlo (GCMC) and molecular dynamics (MD) simulations are performed to investigate the methane aqueous fluids in Na-montmorillonite clay interlayer under near-surface geological temperature and pressure conditions (T = 300 K and P = 20−50 bar). The chemical potentials of water and methane under these T/P conditions are calculated using the Widom's insertion method. These chemical potentials are used in the GCMC simulations to determine the contents of different species in the clay interlayer, especially in those that correspond to the equilibrium stable spacing distances. Simulation results show that initial clay swelling is dominated by water adsorption into the clay interlayer, followed by the intercalation of methane as the basal spacing increases. However, it is found that this methane intercalation process is strongly influenced by the relative humidity and the total gas pressure of the system. High relative humidity may facilitate water molecules entering the clay interlayer region and inhibit the intercalation of methane molecules. MD simulations show that sodium ions are fully hydrated by water molecules and clay surface oxygen atoms, while methane molecules are not fully coordinated. This situation is attributed to the less water content in clay interlayer and the subsequent formation of methane dimer or trimer clusters due to the hydrophobic nature of small hydrocarbon molecules.

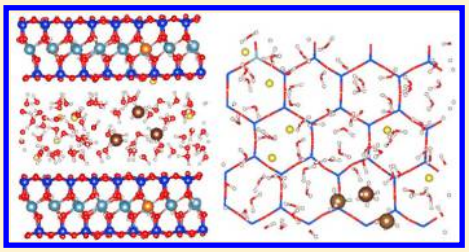

1. INTRODUCTION

Methane aqueous fluid is one type of geological fluids that can form crystalline gas hydrates under specific temperature and pressure (T/P) conditions. The hydrates are clathrate compounds in which methane molecules are enclosed in a cagelike water structure.[1,2] Large amounts of methane hydrate have been found under sediments in permafrost and on the deep ocean floors within specific concentration, temperature, and pressure range. The formation of methane hydrate favors at high pressures and low temperatures, usually occurring in the region with the T/P conditions of approximately 280 K and higher than 3 MPa.[3] Because of the enormous amount, wide geographical distribution, and high energy density of naturally occurring methane hydrates, they are considered as an alternative energy resource capable of contributing to satisfy the world's increasing demand of energy.[4,5] On the other hand, since methane is a potential greenhouse gas, leakage of methane from the hydrates may increase the greenhouse effect and cause further melting of the methane hydrate.[6,7] Inappropriate exploitation of methane hydrate could cause rapid methane hydrate decomposition and possibly induce wellbore instability, landslide, and collapse.[8,9]

The interaction between methane aqueous fluid and clay minerals has been a long-standing interest. Clay minerals are widespread in permafrost and marine sediments. They are phyllosilicates and consist of sheets of silicon−oxygen tetrahedral and sheets of aluminum or magnesium oxygen-hydroxyl octahedral. In particular, aluminum phyllosilicate montmorillonite is one of the best-known and important clay minerals, composed of an aluminum octahedral sheet sandwiched between two silicon tetrahedral sheets. Substitutions of aluminum by magnesium in the octahedral sheet and silicon by aluminum in the tetrahedral sheet could occur and result in negative charges with clay sheets. The neutrality of clay minerals is kept by cations in clay interlayer which have a tendency to be hydrated, leading to clay swelling. Besides water molecules, small hydrocarbon molecules such as methane may also be intercalated into the clay interlayer. While early experimental studies[10,11] did not discriminate methane hydrate formation in clay interlayer or on external clay surfaces, recent experimental investigations[12−14] did show that methane molecules could intercalate into clay interlayer to form clay−methane hydrate intercalate at specific T/P conditions. There have been several molecular simulation studies on the structure and dynamics of methane−water mixture in clay minerals.[15−19] However, the effect of clay on the formation of methane hydrate is still a controversial issue. Previous molecular modeling[15−17] and some experimental results[10,11,14] support the idea that clay minerals promote methane hydrate formation by shifting the stable temperatures of methane hydrate to higher temperatures than those in bulk system. This was observed within experimental T/P conditions of 280−300 K and 20−90 bar pressures. However, other experiments[12,20,21] found that the existence of clay minerals will shift the stable

Received: August 4, 2014
Revised: August 26, 2014
Published: August 28, 2014

temperature of methane hydrate to the lower T relative to that in the bulk methane hydrate. For example, under 30−50 bar pressures, the stable temperatures of methane hydrate in clay will shift downward from those of the bulk methane hydrate by approximately 1−4 K (the corresponding stable T of bulk methane hydrate under the same pressure range are 275−279 K[12]). Recent experiments[14,22,23] also revealed that the methane hydrate formation in clay minerals differs greatly from that in pure methane hydrate. The interlayer cations may significantly influence the methane hydrate stability and decrease cage occupancy of methane due to the entrapment of cations in small cages.

Earlier, Titiloye and Skipper[18,19] investigated the structure and dynamics of methane in clay hydrates under high T/P conditions, corresponding to different burial depths. Under low pressures (<50 atm) and ambient temperature (300 K), Park and Sposito[16] performed Monte Carlo (MC) and molecular dynamics (MD) simulations and found that clay mineral surfaces do have a "thermodynamic promotion effect" on the intercalation of methane hydrates. Cygan et al.[17] even studied much thicker methane hydration layers in montmorillonite clay (approximately six hydration layers) at ambient T/P conditions. Recent simulation studies on the structure of methane, water, and cation system[24] found that the amount and distribution of clay interlayer charges can remarkably affect the behavior of methane hydration.[25] While the actual content of methane and water in clay interlayer could be determined from experimental measurement,[12] a fundamental question concerns how the interface methane hydration layer is formed from the dehydrated state of clay and how the different T/P geological conditions influence the interlayer hydration structure. Our recent molecular simulation studies[26] combining grand-canonical ensemble Monte Carlo (GCMC) and MD simulations revealed that under high T/P (T = 460 K and P = 900 bar) conditions, methane can penetrate into clay interlayer, even at one hydration layer. Initial clay swelling is dominated by water adsorption into clay interlayer, followed by the intercalation of methane as the basal spacing increases. Methane content in clay is found to increase in a stepwise fashion, from initial inner-sphere complex to both inner- and outer-sphere structures.

In our previous studies on the interlayer methane−water mixture under high T/P conditions,[26] only the methane−water binary system was considered in calculating the chemical potentials for each species and the water vapor pressure was assumed to be the saturated vapor pressure. However, methane aqueous geothermal fluids are much more complicated than the simple methane−water binary system. For example, the methane dominated aqueous mixture may contain other hydrocarbon molecules such as ethane and propane, etc.,[10] which will decrease the partial pressure contribution from methane. Meanwhile, the water vapor pressure may not always reach the equilibrium saturated vapor pressure. In this case, the relative humidity (RH) will directly determine the chemical potential of water. Moreover, salinity may influence the solubility of methane in water.[27,28] Geothermal brines may contain many different ions and coions such as Na^+, K^+, Mg^{2+}, Ca^{2+}, Cl^-, and SO_4^{2-}. The partial pressures of water and methane may deviate from those in pure binary mixture. Finally, the capillary pressure[29,30] associated with a broad distribution of pore sizes in natural sediments may change the solubility of methane in water and the phase equilibrium of the aqueous−methane system.[31−34]

The present study will focus on the composition, structure, and dynamics of methane−water hydration layer in clay interlayer when a Na-montmorillonite clay platelet is in contact with a methane-dominated gas mixture. Here we assume that only water and methane molecules have a greater probability to enter the clay interlayer, while other slightly larger hydrocarbon molecules such as ethane and propane, etc. are less likely to enter the clay pore. This assumption would be consistent with early experimental measurements[10] and other molecular simulation studies.[16] The T/P conditions chosen in this work are close to the near-surface geological conditions, setting to the ambient temperature (300 K) and low pressures regime (20−50 bar).[16] These T/P conditions correspond to a burial depth of 130−330 m.[18] Results obtained under these T/P conditions can be used to evaluate the effect of clay surfaces on the formation probability of methane hydrate and to investigate if there is a "shift" of the stable T/P region away from those in the bulk methane hydrates.[12,21]

2. MOLECULAR MODELS AND SIMULATION METHODS

The detailed molecular models and simulation method are given in our previous publication.[26] Essentially, we use the computational packages Towhee[35,36] and LAMMPS[37] to perform GCMC and constant-NVT MD simulations, respectively. The model of clay mineral is the sodium-saturated Wyoming-type montmorillonite that has the chemical formula $Na_{0.75}[Si_{7.75}Al_{0.25}](Al_{3.5}Mg_{0.5})O_{20}(OH)_4$. The clay surfaces contain eight clay unit cells forming a clay patch of 20.77 × 18.03 Å^2. The CLAYFF[38] force field for clay minerals and SPC water model[39] will be used in this simulation work. Methane is represented by the Jorgensen's OPLS all atom (OPLS-AA) model.[40] In MD simulations, the intramolecular bond stretch and bond angle bending terms are introduced into the SPC water model,[41] as well as into the methane molecule,[40] to ensure full flexibility of these molecules and hydroxide components on the clay surface.[38] A cutoff distance of 9.0 Å is used for the dispersive interactions, while the long-range electrostatic interactions are treated by the Ewald summation method.[42]

We choose the T/P conditions of 300 K and 20−50 bar pressure in the simulation. This situation has been studied previously in molecular simulation[16] and experiments[10,11] to investigate the ambient temperature and relatively low-pressure conditions on the clay−methane hydrate interaction. Prior to the GCMC simulations, the chemical potentials of water and methane are computed using the Widom's insertion method for each species in the constant-NPT ensemble Monte Carlo simulations.[43,44] In this ensemble, the temperature is set to the temperature of the mixture, while the pressures for water and methane in methane dominated gas phase are determined based on the relative humidity (RH) and methane volumetric composition of the gas mixture.[10,11] Since methane aqueous fluid contains other species, when studying clay swelling in multicomponent gas mixture, it is more realistic to consider the relative humidity or the partial pressure of water as an important parameter.[45,46] Consequently, the pressure of water (p_w) is determined by its saturated vapor pressure ($p_{w\text{-}sat}$) and relative humidity (i.e., $p_w = p_{w\text{-}sat} \times RH$), while the pressure of methane (p_m) is determined by the total pressure of the gas mixture (p_{tot}) and its volumetric composition, which is set to a specific value of 0.872 in order to be consistent with the experimental setup[10,11] (i.e., $p_m = 0.872\ p_{tot}$). We find that

dx.doi.org/10.1021/jp507884w | J. Phys. Chem. B 2014, 118, 10956−10965

under 300 K and 20−50 bar T/P conditions, methane molecules are incapable of intercalating into the clay interlayer under the saturated water vapor pressure. This is quite different from the cases under high T/P condition (T = 460 K and P = 900 bar at a burial depth of 6 km), in which methane can easily penetrate into the clay interlayer at saturated vapor pressure of water.[26] Therefore, low RH values should be probed under present T/P conditions. Extensive testing shows that RH in the range of 5−30% is a suitable condition to allow for methane intercalating into the clay interlayer. Specifically, the combinations of P = 20 bar and RH = 5−20%, P = 30 bar and RH = 10−20%, or P = 50 bar and RH = 20−30% would be suitable conditions for methane intercalation into the clay pore. Too high RH values beyond the upper bound in both cases will result in predominant water hydration in the clay interlayer. On the other hand, too low RH values (<5%) and pressures (<20 bar) will have less water and methane entering the clay interlayer.

The GCMC simulation is performed at each clay pore size for at least 10 million moves, which include insertion and deletion, as well as translation and rotation of molecules. The virial pressure perpendicular to the clay interface for the confined methane aqueous system is calculated in Towhee[35,36] and will be compared with external pressure to find the equilibrium interlayer spacing. Subsequent NVT MD simulations are performed in LAMMPS[37] to study the structure and dynamics of the confined methane aqueous fluids at equilibrium spacing distances. The MD simulation time usually takes 5 ns in production run with a time step of 1 fs for the data collection to obtain the related thermodynamic properties.

3. RESULTS AND DISCUSSION

3.1. Grand Canonical Monte Carlo Simulation: Equilibrium Stable Methane Aqueous Fluids in Clay Interlayer. We first perform GCMC simulations to study the clay swelling in the water vapor environment. Two RH values, a very low relative humidity (8.9%), and a very high relative humidity (67%) are selected to compare with the previously published results by Tambach et al.[45] The chemical potentials of water corresponding to these two RH values are computed as −51.06 kJ/mol and −46.05 kJ/mol, respectively. It is noted that the chemical potential of water at saturated vapor phase (RH = 100%) is −45.56 kJ/mol.[26] Figure 1 shows the variations of the pressures normal to the clay sheets (P_z) as a function of basal spacing from our simulations. The pressure ∼ basal spacing curves compare reasonably well with Tambach et al.'s results, in which the normal pressure is calculated by the trial volume method.[45]

With the confidence of the virial pressure calculations, we are able to find the equilibrium basal spacing of clay interlayer at different T/P and RH conditions in the methane-dominated gas phase. We perform the GCMC simulations to study the clay swelling in the methane aqueous mixture at T = 300 K and P = 20, 30, or 50 bar pressure conditions. Specific RH values are considered in each case: RH = 5%, 10%, and 20% for T/P = 300 K/20 bar; RH = 10% and 20% for T/P = 300 K/30 bar; and RH = 20% and 30% for T/P = 300 K/50 bar. The chemical potentials of water and methane under these seven different thermodynamic conditions are obtained from Widom's insertion method through the constant-NPT ensemble Monte Carlo simulations and are given in Table 1. Note that the chemical potential of water vapor only depends on T and RH, while the chemical potential of methane only depends on T/P.

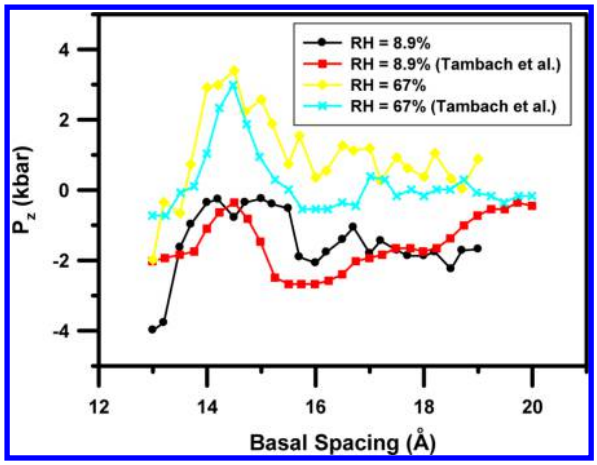

Figure 1. Variation of normal pressure (P_z) as a function of the basal spacing of Na-montmorillonite clay under two relative humidity values (RH) of 8.9% and 67%. For comparison, previous simulation results by Tambach et al.[45] are also included.

Table 1. Chemical Potentials of Water and Methane in the Gas Mixture Under Seven Different T/P and RH Conditions

T, P, and RH (%)	chemical potential of water (kJ/mol)	chemical potential of methane (kJ/mol)
300 K, 20 bar, 5	−53.08 ± 0.01	−28.01 ± 0.02
300 K, 20 bar, 10	−51.35 ± 0.04	−28.01 ± 0.02
300 K, 20 bar, 20	−49.63 ± 0.05	−28.01 ± 0.02
300 K, 30 bar, 10	−51.35 ± 0.04	−27.02 ± 0.02
300 K, 30 bar, 20	−49.63 ± 0.05	−27.02 ± 0.02
300 K, 50 bar, 20	−49.63 ± 0.05	−25.80 ± 0.03
300 K, 50 bar, 30	−48.62 ± 0.03	−25.80 ± 0.03

As the RH value is increased, the chemical potential of water is also increased.

A series of GCMC simulations involving at least 10 million moves of molecules are performed with various basal spacing from 13 to 24 Å. These GCMC runs are followed by 30-million-move continuing runs to get statistic values for water and methane contents. The pressure normal to the clay interface as a function of basal spacing is shown in Figure 2.

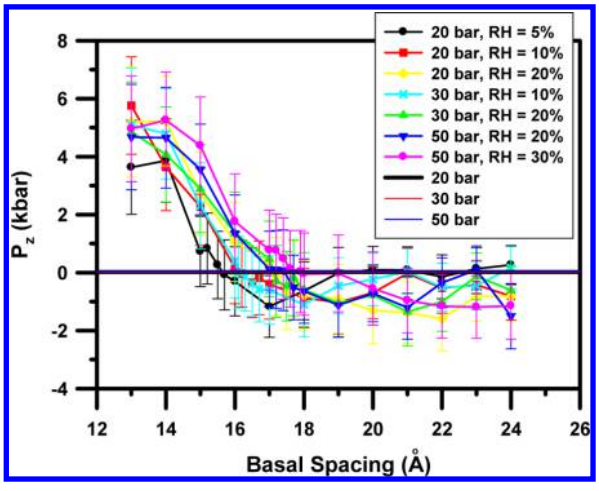

Figure 2. Variations of normal pressure (P_z) as a function of the basal spacing of Na-montmorillonite clay under seven different T/P/RH conditions. The three horizontal lines at 20, 30, and 50 bar pressures overlap near zero pressure line.

dx.doi.org/10.1021/jp507884w | J. Phys. Chem. B 2014, 118, 10956−10965

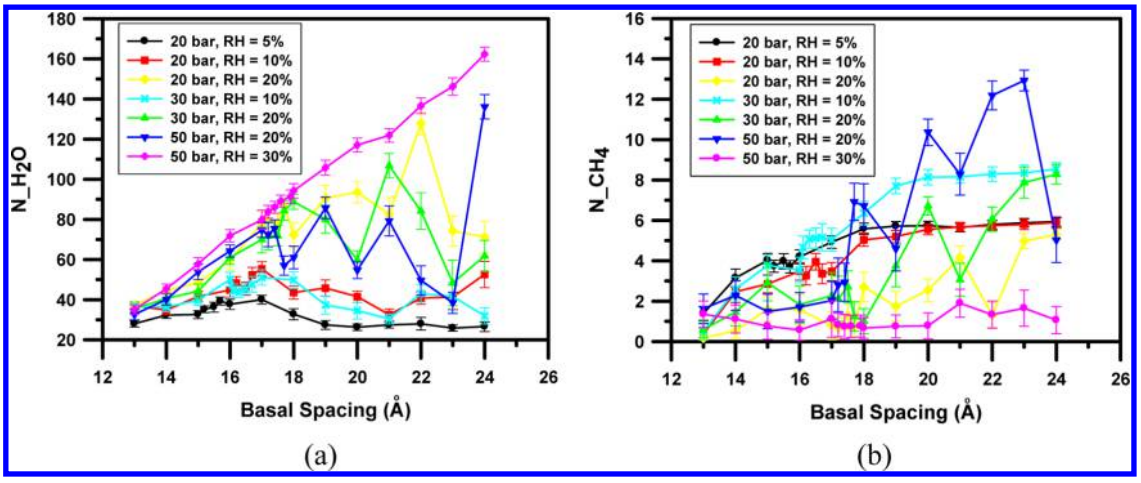

Figure 3. Average number of (a) water and (b) methane molecules entering the clay interlayer.

The three horizontal lines close to zero represent the three external bulk pressures of 20, 30, and 50 bar, respectively. The equilibrium basal spacing in each of seven T/P/RH cases corresponds to the intersections between the negative slope part of the normal pressure curve and the horizontal external pressure line. The confined methane aqueous fluids in these basal spacing distances are thermodynamically stable that correspond to free energy minima.[45] Figure 2 shows that the equilibrium basal spacing increases with both pressure P and RH, indicating that higher pressure (P) and higher relative humidity (RH) promote more methane and water molecules intercalated into the clay interlayer.

Figure 3 shows the average numbers of water and methane molecules entering the clay interlayer as a function of basal spacing. The figure shows that at 13 Å basal spacing, which already incorporates at least one layer of water molecules in all seven T/P/RH cases, very few methane molecules could penetrate into the clay interlayer. The initial clay swelling is largely dominated by water adsorption. This result is similar to the case under high T/P conditions we previously reported.[26] As the basal spacing is increased, it is clearly seen that the competition of water and methane entering the clay interlayer strongly depends on the relative humidity. Higher relative humidity facilitates more water molecules entering the clay interlayer, resulting in less methane content. For the same relative humidity (e.g., RH = 20%), higher pressure of gas mixture usually leads to more methane intercalated into clay, simply because the partial pressure of methane (p_m) is proportional to the total pressure of the mixture (p_{tot}). However, fluctuations in water and methane contents are seen with varying basal spacing at RH = 20%. The increasing of water content with basal spacing is accompanied by the decreasing of methane content and vice versa. In the case of 30 bar and 10% RH, the low relative humidity allows for more methane being intercalated into the clay interlayer (up to 8 methane molecules in the simulation box), while the number of water molecules fluctuates around 30−40. In the other extreme case, at 50 bar pressure and 30% RH, the relatively high RH makes water content increasing almost proportionally with basal spacing, while the number of methane molecules remains at a very low level around 1.0 in the whole range of basal spacing.

Since the normal pressure curve may have multiple stable intersections with the horizontal external pressure line (see Figure 2) and the first stable spacing is the most possible clay swelling distance,[45] in the present study we only focus on the first stable methane−water clay hydrate. Table 2 summarizes the stable clay spacing and the corresponding water and methane contents in the Wyoming-type montmorillonite clay interlayer.

Table 2. Equilibrium Basal Spacing, Water and Methane Contents under the Seven T/P/RH Cases in Wyoming-Type Montmorillonite Clay

T, P, and RH (%)	equil. basal spacing (Å)	n_{H_2O}	n_{CH_4}
300 K, 20 bar, 5	15.5	36	4
300 K, 20 bar, 10	16.0	45	3
300 K, 20 bar, 20	17.0	78	1
300 K, 30 bar, 10	16.1	44	5
300 K, 30 bar, 20	17.0	70	2
300 K, 50 bar, 20	17.4	75	3
300 K, 50 bar, 30	17.9	91	1

As an additional comparison with the previous simulation work by Park and Sposito,[16] we have recalculated water and methane content at 19.4 Å basal spacing (corresponding to three hydration layers) under P = 20 bar pressure. For RH = 5−20% relative humidity, the water content in clay interlayer gradually increases as methane content decreases. However, none of these cases can reach a relatively high loading level of methane with high water content. These results are summarized in Table 3.

3.2. Molecular Dynamics Simulation: Structure and Dynamics of Methane Aqueous Fluids in Clay Interlayer.

Methane−Water−Cation Hydration Structure in Clay Interlayer. Molecular dynamics (MD) simulations based on

Table 3. Water and Methane Contents at 19.4 Å Basal Spacing from Different Simulation Results

basal spacing (Å)	pressure (bar)	RH (%)	n_{H_2O}	n_{CH_4}
19.4	20	5	29	6
19.4	20	10	42	5
19.4	20	20	106	1
19.4[a]	20	–	88	8

[a]Simulation work by Park and Sposito.[16]

dx.doi.org/10.1021/jp507884w | J. Phys. Chem. B 2014, 118, 10956−10965

the seven GCMC equilibrium basal spacing configurations (Table 2) are further performed to investigate the structure and dynamics of the intercalated methane−water mixture. The density profiles of methane in the interlayer region are shown in Figure 4. In all the seven cases in which the basal spacing

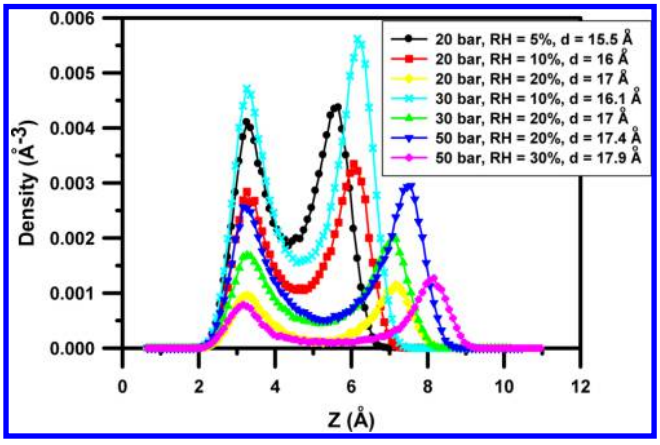

Figure 4. Density profiles of methane (represented by the carbon atom, C_m, in methane molecule) in the interlayer region. The origin corresponds to the clay surface oxygen.

varies from 15.5−17.9 Å, methane exhibits two distinct peaks close to the two clay surfaces, indicating that methane has a strong affinity to the clay surface and can form inner-sphere hydrate.[15] Water density distributions (Figure 5) in these

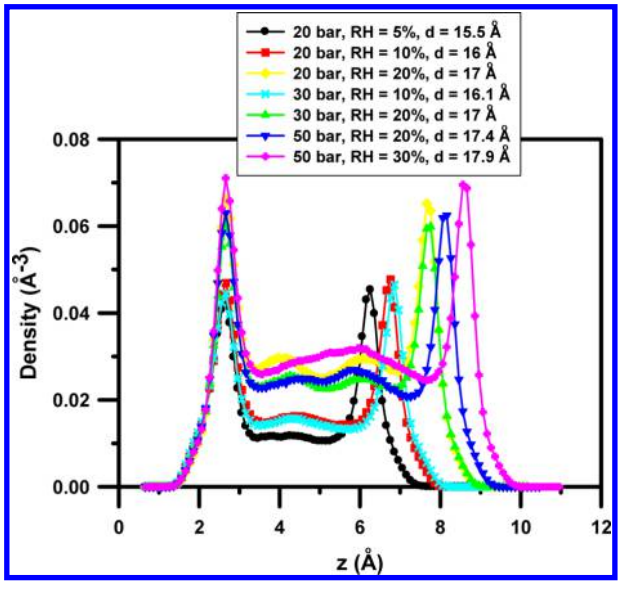

Figure 5. Density profiles of water (represented by water oxygen, O_w) in the interlayer region. The origin corresponds to the clay surface oxygen.

equilibrium basal spacing distances also exhibit two distinct peaks near clay surfaces. In the central region, they remain relatively flat but increase as the water content increases. The density distribution of water in this central region is also mediated by the hydrated sodium cations which will be discussed below.

Figure 6 shows the density profiles of sodium cations in the interlayer region. We find that these distribution curves strongly depend on the RH values. At low relative humidity of 5% and

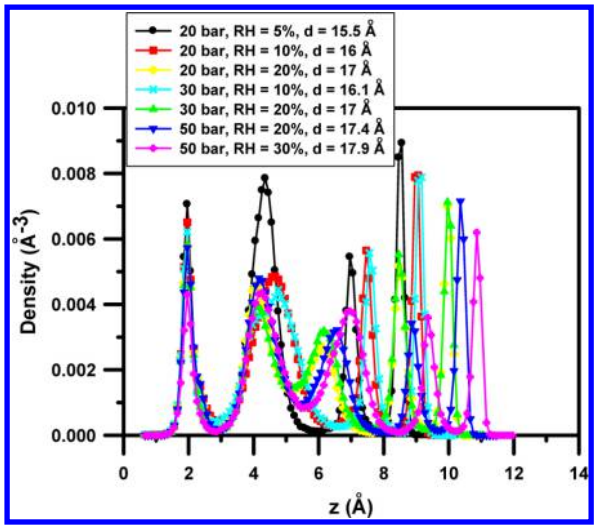

Figure 6. Density profiles of sodium ions in the interlayer region. The origin corresponds to the clay surface oxygen.

10% cases with smaller basal spacing (15.5−16.1 Å), sodium ions only show four distinct hydration peaks. At relatively high humidity of 20% and 30% with larger basal spacing (17−17.9 Å), they have increased to five distinct hydration peaks. The latter cases are also similar to those under high T/P condition in our previous work.[26] The asymmetric distribution of Na^+ cations between two clay surfaces is largely due to the unevenly distributed surface charges on clay surfaces. These hydrated cations close to clay surfaces form the inner-sphere complexes, while cations in the central peak region form outer-sphere hydration complexes.[15]

We have further calculated the radial distribution functions (RDFs) for methane−water (CH_4−O_w) and methane−surface oxygen (CH_4−O_s) to investigate methane hydration structure. The results are presented in Figure 7, panels a and b. The partial CH_4−O_w and CH_4−O_s and the total coordination number of water around methane are listed in Table 4, which are calculated by integrating the RDFs to the first minimum.

From Table 4 it is clearly seen that all of the methane−oxygen coordination numbers in clay interlayer are smaller than that when methane is in bulk water. This is particularly outstanding at 15.5, 16.0, and 16.1 Å basal spacing when the clay interlayer contains 3−5 methane molecules, for which the coordination number is reduced by roughly 55% compared to the bulk value. This phenomenon is also seen at high T/P conditions[26] but less severe than the low T/P conditions studied here. To understand the origin of this very low methane coordination number in the clay interlayer, we have further calculated the RDFs of methane−methane and sodium−oxygen pairs. In Figure 7, the remaining three panels (c, d, and e) show the methane−methane (CH_4−CH_4), sodium−water (Na^+−O_w), and sodium−surface oxygen (Na^+−O_s) RDF curves. The first CH_4−CH_4 RDF peak is located at a distance of 4.0 Å, which is comparable to the distance of the CH_4−O_w or CH_4−O_s pair. This further indicates that methane molecules are not fully coordinated by water molecules. Rather, they tend to form methane dimer or small cluster due to the hydrophobic nature of methane. In contrast, sodium ions are fully hydrated by water molecules and clay surface oxygen in the clay interlayer. Table 5 shows the partial Na^+−O_w and Na^+−O_s, as well as the total oxygen coordination number for Na^+ in the seven MD simulation cases. The total oxygen coordination numbers for

dx.doi.org/10.1021/jp507884w | J. Phys. Chem. B 2014, 118, 10956−10965

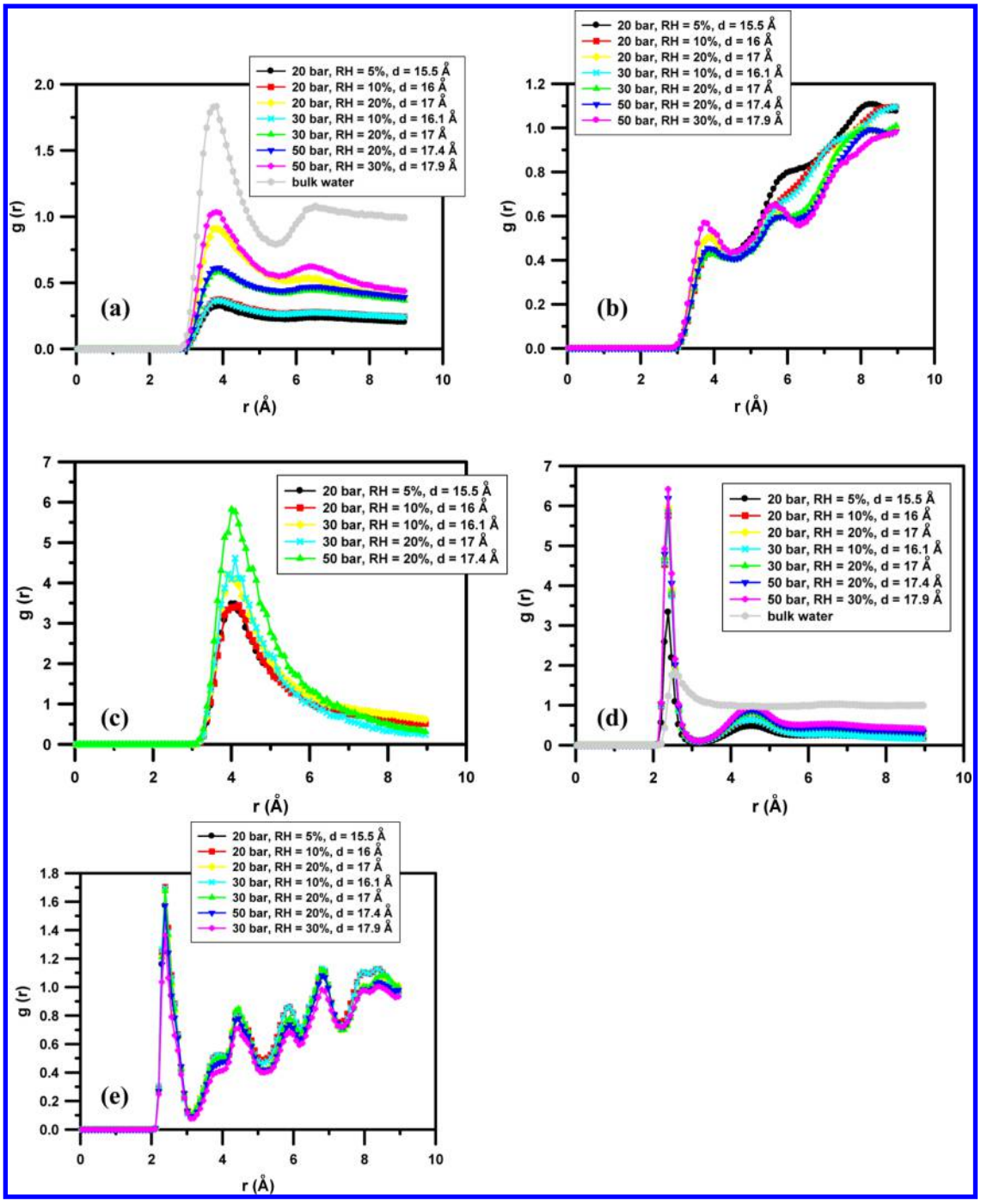

Figure 7. Radial distribution functions of (a) CH_4−O_w; (b) CH_4−O_s; (c) CH_4−CH_4; (d) Na^+−O_w; and (e) Na^+−O_s interaction pairs at 300 K with different *P*, RH, and basal spacing *d* values. The functions are normalized by the density of bulk water at 300 K and 1 bar of pressure.

Na^+ in each case is around 6, the same hydration number of sodium ion in bulk water.[47]

Figure 8 shows the typical snapshots of methane aqueous hydration configurations in two MD simulation cases. The first case corresponds to the equilibrium basal spacing of 17 Å, with *P* = 30 bar and RH = 20%, which contains 2 methane molecules. The second case corresponds to the equilibrium basal spacing of 17.4 Å, with *P* = 50 bar and RH = 20%, which contains 3 methane molecules. Methane aqueous hydration structures in the other five MD simulation cases are shown in Figure S1 (see the Supporting Information). These snapshots clearly show the formations of the methane dimer (Figure 8a) or trimer (Figure 8b) when multiple methane molecules are intercalated into the clay interlayer.

To further give insight into the hydration structure of the methane−water−ion complex in the clay interlayer, in Figure 9, we plot the two-dimensional (2D) density distributions of methane, sodium ion (Na^+), and water molecules projected onto the lateral *xy* plane for the two simulation cases (i.e., 17 Å spacing/*P* = 30 bar/RH = 20% and 17.4 Å spacing/*P* = 50 bar/RH = 20%). The lateral density distributions of different species in the other 5 cases are shown in Figure S2 of the Supporting Information. There are essentially two interesting observations shown in the figure. The first is that methane

dx.doi.org/10.1021/jp507884w | J. Phys. Chem. B 2014, 118, 10956−10965

Table 4. Coordination Numbers of Water and Clay Oxygen around Methane at T = 300 K and P = 20−50 bar with Different RH Values

basal spacing (Å)	pressure (bar)	RH (%)	n_{CH_4-Ow}	$n_{CH_4-O_s}$	n_t[a]
15.5	20	5	5.4	2.8	8.2
16.0	20	10	6.7	2.6	9.3
17.0	20	20	14.0	3.8	17.8
16.1	30	10	6.3	3.0	9.3
17.0	30	20	9.5	3.0	12.5
17.4	50	20	9.9	3.1	13.0
17.9	50	30	13.7	3.3	17.0
bulk water	1	100	20.7	–	20.7

[a] n_t is the total coordination number of oxygen around methane.

Table 5. Coordination Number of Water and Clay Oxygen around Sodium Ion at T = 300 K and P = 20−50 bar with Different RH Values

basal spacing (Å)	pressure (bar)	RH (%)	n_{Na-O_w}	n_{Na-O_s}	n_t[a]
15.5	20	5	4.4	1.6	6.0
16.0	20	10	4.1	1.9	6.0
17.0	20	20	4.3	1.7	6.0
16.1	30	10	4.1	1.9	6.0
17.0	30	20	4.2	1.7	5.9
17.4	50	20	4.4	1.6	6.0
17.9	50	30	4.6	1.4	6.0
bulk water	1	100	6.0	–	6.0

[a] n_t is the total coordination number of oxygen around sodium.

molecules and Na^+ ions are situated in two distinct regions. These two regions are mutually supplementary in the xy plane. The second is that the 2D density distribution of water molecules essentially coincides with the sodium region, indicating that Na^+ ions are fully hydrated by water molecules (plus the clay surface oxygen atoms) in the clay interlayer. This result is consistent with our previous discussion. Since the Na^+ ion has a larger hydration energy than methane and methane is hydrophobic in nature, the combined two effects will essentially deplete methane hydrate if it does exist in the clay interlayer, at least under the current T/P conditions. The fact that Na^+ alkali metal ion has a larger hydration energy than the dissociation enthalpy of the methane hydrate can also explain experimental observation of cavity occupancy by sodium cations in sediment methane hydrates.[22,23]

Diffusion Behaviors of Different Species in Clay Interlayer. To understand the dynamics behavior of methane aqueous fluid in the clay interlayer, we calculate the 2D self-diffusion coefficients of methane, water, and sodium ions in the seven simulation cases. The calculation method is described in our previous publication.[26] The results are tabulated in Table 6. The 3D diffusion coefficients of these different species in bulk water and those obtained by Park and Sposito[16] are also included in the table for comparison. In general, the diffusion coefficients of water are smaller than the bulk value due to the confinement effect of clay surfaces. On the other hand, it is seen that in most cases the diffusion coefficients of methane under different T/P/RH conditions are larger than those of water molecules. We attribute this very high mobility of methane to the less hydrated environment in the clay interface. Since the diffusion coefficients of methane, water, and sodium ions are comparable to those in bulk liquid water in all of the simulation cases (see Table 6), the fluidic behavior of methane aqueous

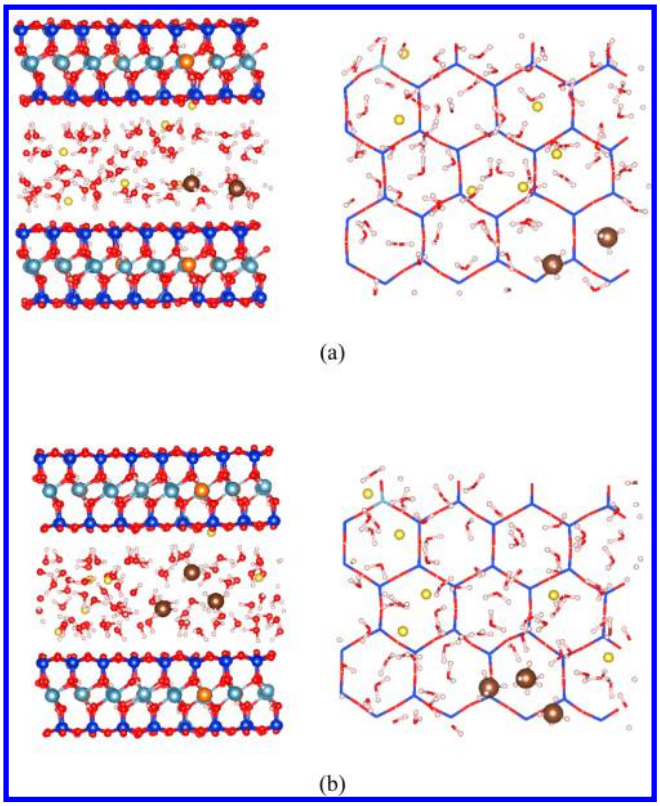

Figure 8. Snapshots of methane aqueous hydration structure in the Na−montmorillonite interlayer in two T/P/RH simulation cases. The left and right panels show the side and top views of the molecular configurations. (a) T/P/RH = 300 K/30 bar/20%, equilibrium basal spacing = 17 Å; (b) T/P/RH = 300 K/50 bar/20%, equilibrium basal spacing = 17.4 Å. Color scheme: oxygen, red; hydrogen, white; carbon, brown; silicon, blue; aluminum, cyan; magnesium, orange; and sodium, yellow.

system in the clay interlayer will prevent the formation of crystalline methane hydrate under the T/P conditions studied here.

Given the fact that nanoconfined water is always fluidic,[52−54] while the hydrated metal ions has a load bearing capacity,[55,56] we anticipate that even though methane has a higher mobility than water and sodium ions in clay interlayer, the methane−water−ion complex will still be able to produce strong repulsive hydration force to balance external pressure, which is similar to the scenario of mica surfaces in an aqueous electrolyte solution.[56]

The T/P conditions we studied here are close to the upper-temperature stability region for the formation of methane hydrate ice crystal.[10−12,14,16,21] Therefore, it is not surprising that the methane−water−cation complex in the clay interlayer is highly fluidic. A lower temperature regime should be explored in future work to investigate how likely the solid crystalline structure of methane hydrate could be formed in clay interlayer.

4. CONCLUSIONS

In the present work, the structure and dynamics of methane aqueous fluid in a Na−montmorillonite clay interlayer under near-surface T/P conditions have been studied through the GCMC and MD simulations. On the basis of previous experimental data of the composition of typical methane gas mixture, the chemical potentials of methane and water in gas

dx.doi.org/10.1021/jp507884w | J. Phys. Chem. B 2014, 118, 10956−10965

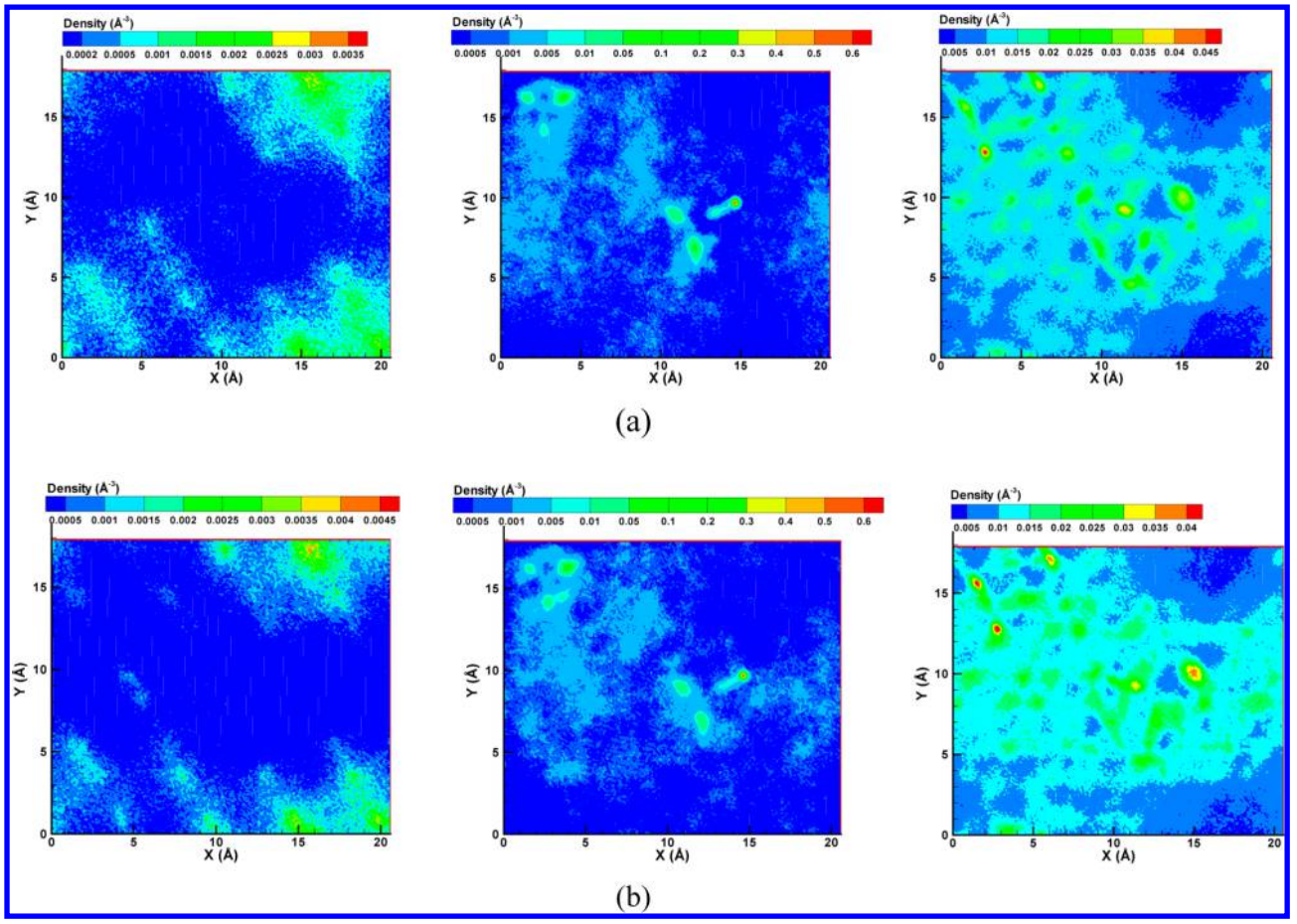

Figure 9. In-plane two-dimensional (2D) density distributions of methane (left), sodium ions (middle), and water molecules (right) in the clay interlayer under two typical simulation conditions: (a) $T/P/RH$ = 300 K/30 bar/20% at an equilibrium basal spacing of 17 Å and (b) $T/P/RH$ = 300 K/50 bar/20% at an equilibrium basal spacing of 17.4 Å.

Table 6. Diffusion Coefficients of Methane, Water, and Sodium Ions in Clay Interlayer under T = 300 K and P = 20−50 bar with Different RH Values

basal spacing (Å)	pressure (bar)	RH (%)	D_{CH_4} ($\times 10^{-9}$ m^2/s)	D_{H_2O} ($\times 10^{-9}$ m^2/s)	D_{Na} ($\times 10^{-9}$ m^2/s)
15.5	20	5	13.55	0.84	0.15
16.0	20	10	9.59	1.33	0.20
17.0	20	20	3.12	1.82	0.28
16.1	30	10	11.28	1.24	0.24
17.0	30	20	0.82	1.73	0.36
17.4	50	20	1.84	1.72	0.39
17.9	50	30	2.63	2.03	0.60
18.53[a]	10	–	1.135	1.955	0.14
19.40[a]	20	–	2.319	1.676	0.13
bulk liquid water	–	–	1.49[b] (2.52[c])	2.3[d]	0.20[e]

[a]Simulation work by Park and Sposito.[16] [b]Experimental result at 298 K.[48] [c]Simulation work by Alavi and Ripmeester.[49] [d]Experimental result at 298 K.[50] [e]Experimental result at 298 K.[51]

mixture are calculated by the Widom's insertion method. The GCMC simulations are then performed to determine the equilibrium basal spacing distances under different $T/P/RH$ conditions. We find that there is a competition of surface sorption between water and methane molecules. The initial clay swelling is dominated by water adsorption. However, during the subsequent clay swelling, this surface sorption competition critically depends on the relative humidity and the pressure of the gas mixture. Higher relative humidity and lower gas pressure facilitate water molecules entering the clay interlayer and inhibit the intercalation of methane molecules, while lower relative humidity and higher gas pressure will allow more methane molecules to enter the clay interlayer.

The density distributions of methane from MD simulations show that methane has a strong affinity for clay surfaces. The radial distribution function and coordination calculations show that sodium ions are fully hydrated in the clay interlayer, while methane molecules are much less coordinated by water molecules. The methane−methane pair correlation functions and the snapshots of methane aqueous configurations clearly

dx.doi.org/10.1021/jp507884w | J. Phys. Chem. B 2014, 118, 10956−10965

show the formation of methane dimer or trimer clusters due to the hydrophobic nature of methane molecules. The present study shows that under the near-surface T/P/RH conditions, the diffusion coefficients of different species in the clay interlayer are comparable to their counterparts in the bulk fluids. Methane aqueous fluids in the clay interlayer are quite fluidic and will not be able to solidify into ice crystals. Therefore, the lower temperature regime should be further investigated to see how likely the clay minerals may shift the stable T/P region away from those in the bulk methane hydrates.[12,21]

■ ASSOCIATED CONTENT

Supporting Information

This information contains snapshots of methane aqueous fluids in montmorillonite clay interlayer (Figure S1) and the corresponding 2D density distributions of different species projected onto the *xy* plane (Figure S2) from other five simulation cases. This material is available free of charge via the Internet at http://pubs.acs.org.

■ AUTHOR INFORMATION

Corresponding Author

*E-mail: leng@gwu.edu. Tel: 202-994-5964.

Notes

The authors declare no competing financial interest.

■ ACKNOWLEDGMENTS

This work is supported by the American Chemical Society Petroleum Research Fund (PRF no. 49596-DNI 5) and the National Energy Research Scientific Computing Center (NERSC).

■ REFERENCES

(1) Sloan, E. D.; Koh, C. *Clathrate Hydrates of Natural Gases*; CRC Press: Boca Raton, FL, 2007.
(2) Sloan, E. D. Gas Hydrates: Review of Physical/Chemical Properties. *Energy Fuels* **1998**, *12*, 191−196.
(3) Kvenvolden, K. A. Potential Effects of Gas Hydrate on Human Welfare. *Proc. Natl. Acad. Sci. U.S.A.* **1999**, *96*, 3420−3426.
(4) Kvenvolden, K. A. Methane Hydrate: A Major Reservoir of Carbon in the Shallow Geosphere. *Chem. Geol.* **1988**, *71*, 41−51.
(5) Milkov, A. V.; Sassen, R. Economic Geology of Offshore Gas Hydrate Accumulations and Provinces. *Mar. Pet. Geol.* **2002**, *19*, 1−11.
(6) Bains, S.; Corfield, R. M.; Norris, R. D. Mechanisms of Climate Warming at the End of the Paleocene. *Science* **1999**, *285*, 724−727.
(7) Archer, D.; Buffett, B.; Brovkin, V. Ocean Methane Hydrates as a Slow Tipping Point in the Global Carbon Cycle. *Proc. Natl. Acad. Sci. U.S.A.* **2009**, *106*, 20596−20601.
(8) Sultan, N.; Cochonat, P.; Foucher, J. P.; Mienert, J. Effect of Gas Hydrates Melting on Seafloor Slope Instability. *Mar. Geol.* **2004**, *213*, 379−401.
(9) Nisbet, E. G.; Piper, D. J. W. Giant Submarine Landslides. *Nature* **1998**, *392*, 329−330.
(10) Cha, S. B.; Ouar, H.; Wildeman, T. R.; Sloan, E. D. A 3rd-Surface Effect on Hydrate Formation. *J. Phys. Chem.* **1988**, *92*, 6492−6494.
(11) Ouar, H.; Cha, S. B.; Wildeman, T. R.; Sloan, E. D. The Formation of Natural-Gas Hydrates in Water-Based Drilling-Fluids. *Chem. Eng. Res. Des.* **1992**, *70*, 48−54.
(12) Guggenheim, S.; van Groos, A. F. K. New Gas-Hydrate Phase: Synthesis and Stability of Clay-Methane Hydrate Intercalate. *Geology* **2003**, *31*, 653−656.
(13) van Groos, A. F. K.; Guggenheim, S. The Stability of Methane Hydrate Intercalates of Montmorillonite and Nontronite: Implications for Carbon Storage in Ocean-Floor Environments. *Am. Mineral.* **2009**, *94*, 372−379.
(14) Seo, Y. J.; Seol, J.; Yeon, S. H.; Koh, D. Y.; Cha, M. J.; Kang, S. P.; Seo, Y. T.; Bahk, J. J.; Lee, J.; Lee, H. Structural, Mineralogical, and Rheological Properties of Methane Hydrates in Smectite Clays. *J. Chem. Eng. Data* **2009**, *54*, 1284−1291.
(15) Sposito, G.; Skipper, N. T.; Sutton, R.; Park, S. H.; Soper, A. K.; Greathouse, J. A. Surface Geochemistry of the Clay Minerals. *Proc. Natl. Acad. Sci. U.S.A.* **1999**, *96*, 3358−3364.
(16) Park, S. H.; Sposito, G. Do Montmorillonite Surfaces Promote Methane Hydrate Formation? Monte Carlo and Molecular Dynamics Simulations. *J. Phys. Chem. B* **2003**, *107*, 2281−2290.
(17) Cygan, R. T.; Guggenheim, S.; van Groos, A. F. K. Molecular Models for the Intercalation of Methane Hydrate Complexes in Montmorillonite Clay. *J. Phys. Chem. B* **2004**, *108*, 15141−15149.
(18) Titiloye, J. O.; Skipper, N. T. Molecular Dynamics Simulation of Methane in Sodium Montmorillonite Clay Hydrates at Elevated Pressures and Temperatures. *Mol. Phys.* **2001**, *99*, 899−906.
(19) Titiloye, J. O.; Skipper, N. T. Monte Carlo and Molecular Dynamics Simulations of Methane in Potassium Montmorillonite Clay Hydrates at Elevated Pressures and Temperatures. *J. Colloid Interface Sci.* **2005**, *282*, 422−427.
(20) Kotkoskie, T.; Al-Ubaidi, B.; Wildeman, T.; Sloan, E. Inhibition of Gas Hydrates in Water-Based Drilling Muds. *SPE Drilling Engineering* **1992**, *7*, 130−136.
(21) Lu, H. L.; Matsumoto, R. Preliminary Experimental Results of the Stable P-T Conditions of Methane Hydrate in a Nannofossil-Rich Claystone Column. *Geochem. J.* **2002**, *36*, 21−30.
(22) Yeon, S. H.; Seol, J.; Seo, Y. J.; Park, Y.; Koh, D. Y.; Park, K. P.; Huh, D. G.; Lee, J.; Lee, H. Effect of Interlayer Ions on Methane Hydrate Formation in Clay Sediments. *J. Phys. Chem. B* **2009**, *113*, 1245−1248.
(23) Yeon, S. H.; Seol, J.; Koh, D. Y.; Seo, Y. J.; Park, K. P.; Huh, D. G.; Lee, J.; Lee, H. Abnormal Methane Occupancy of Natural Gas Hydrates in Deep Sea Floor Sediments. *Energy Environ. Sci.* **2011**, *4*, 421−424.
(24) Zhang, J. F.; Choi, S. K. Molecular Dynamics Simulation of Methane in Potassium Montmorillonite Clay Hydrates. *J. Phys. B: At., Mol. Opt. Phys.* **2006**, *39*, 3839−3848.
(25) Zhou, Q.; Lu, X. C.; Liu, X. D.; Zhang, L. H.; He, H. P.; Zhu, J. X.; Yuan, P. Hydration of Methane Intercalated in Na-Smectites with Distinct Layer Charge: Insights from Molecular Simulations. *J. Colloid Interface Sci.* **2011**, *355*, 237−242.
(26) Rao, Q.; Xiang, Y.; Leng, Y. S. Molecular Simulations on the Structure and Dynamics of Water-Methane Fluids between Na-Montmorillonite Clay Surfaces at Elevated Temperature and Pressure. *J. Phys. Chem. C* **2013**, *117*, 14061−14069.
(27) Duan, Z. H.; Moller, N.; Greenberg, J.; Weare, J. H. The Prediction of Methane Solubility in Natural-Waters to High Ionic-Strength from 0-Degrees-C to 250-Degrees-C and from 0 to 1600 bar. *Geochim. Cosmochim. Acta* **1992**, *56*, 1451−1460.
(28) Duan, Z. H.; Mao, S. D. A Thermodynamic Model for Calculating Methane Solubility, Density and Gas Phase Composition of Methane-Bearing Aqueous Fluids from 273 to 523 K and from 1 to 2000 bar. *Geochim. Cosmochim. Acta* **2006**, *70*, 3369−3386.
(29) Jain, A. K.; Juanes, R. Preferential Mode of Gas Invasion in Sediments: Grain-Scale Mechanistic Model of Coupled Multiphase Fluid Flow and Sediment Mechanics. *J. Geohys. Res.* **2009**, *114*, 19.
(30) Salimi, H.; Wolf, K. H.; Bruining, J. The Influence of Capillary Pressure on the Phase Equilibrium of the CO_2-Water System: Application to Carbon Sequestration Combined with Geothermal Energy. *Int. J. Greenhouse Gas Control* **2012**, *11*, S47−S66.
(31) Ben Clennell, M.; Hovland, M.; Booth, J. S.; Henry, P.; Winters, W. J. Formation of Natural Gas Hydrates in Marine Sediments 1. Conceptual Model of Gas Hydrate Growth Conditioned by Host Sediment Properties. *J. Geophys. Res.* **1999**, *104*, 22985−23003.
(32) Henry, P.; Thomas, M.; Ben Clennell, M. Formation of Natural Gas Hydrates in Marine Sediments 2. Thermodynamic Calculations of

Stability Conditions in Porous Sediments. *J. Geophys. Res.* **1999**, *104*, 23005−23022.
(33) Ben Clennell, M.; Henry, P.; Hovland, M.; Booth, J. S.; Winters, G. J.; Thomas, M. Formation of Natural Gas Hydrates in Marine Sediments: Gas Hydrate Growth and Stability Conditioned by Host Sediment Properties. In *Gas Hydrates: Challenges for the Future*, Holder, G. D., Bishnoi, P. R., Eds.; New York Academy of Sciences: New York, 2000; Vol. *912*, pp 887−896.
(34) Pesaran, A.; Shariati, A. Effect of Capillary Term Parameters on the Thermodynamic Modeling of Methane Hydrate Formation in Porous Media. *J. Nat. Gas Sci. Eng.* **2013**, *14*, 192−203.
(35) Martin, M. G.; Siepmann, J. I. Transferable Potentials for Phase Equilibria. 1. United-Atom Description of N-Alkanes. *J. Phys. Chem. B* **1998**, *102*, 2569−2577.
(36) Martin, M. G.; Siepmann, J. I. Novel Configurational-Bias Monte Carlo Method for Branched Molecules. Transferable Potentials for Phase Equilibria. 2. United-Atom Description of Branched Alkanes. *J. Phys. Chem. B* **1999**, *103*, 4508−4517.
(37) Plimpton, S. Fast Parallel Algorithms for Short-Range Molecular-Dynamics. *J. Comput. Phys.* **1995**, *117*, 1−19.
(38) Cygan, R. T.; Liang, J. J.; Kalinichev, A. G. Molecular Models of Hydroxide, Oxyhydroxide, and Clay Phases and the Development of a General Force Field. *J. Phys. Chem. B* **2004**, *108*, 1255−1266.
(39) Berendsen, H. J. C., Postma, J. P. M.; van Gunsteren, W. F.; Hermans, J. Interaction Models for Water in Relation to Protein Hydration. In *Intermolecular Forces*, Pullman, B., Ed.; D. Reidel: Amsterdam, 1981; p 331.
(40) Jorgensen, W. L.; Maxwell, D. S.; TiradoRives, J. Development and Testing of the Opls All-Atom Force Field on Conformational Energetics and Properties of Organic Liquids. *J. Am. Chem. Soc.* **1996**, *118*, 11225−11236.
(41) Teleman, O.; Jonsson, B.; Engstrom, S. A Molecular-Dynamics Simulation of a Water Model with Intramolecular Degrees of Freedom. *Mol. Phys.* **1987**, *60*, 193−203.
(42) Allen, M. P., Tildesley, D. J. *Computer Simulation of Liquids*; Clarendon Press: Oxford, 1987.
(43) Widom, B. Some Topics in the Theory of Fluids. *J. Chem. Phys.* **1963**, *39*, 2802−2812.
(44) Frenkel, D., Smit, B. *Understanding Molecular Simulation*; Academic Press: New York, 1996.
(45) Tambach, T. J.; Hensen, E. J. M.; Smit, B. Molecular Simulations of Swelling Clay Minerals. *J. Phys. Chem. B* **2004**, *108*, 7586−7596.
(46) Tambach, T. J.; Bolhuis, P. G.; Hensen, E. J. M.; Smit, B. Hysteresis in Clay Swelling Induced by Hydrogen Bonding: Accurate Prediction of Swelling States. *Langmuir* **2006**, *22*, 1223−1234.
(47) Jensen, K. P.; Jorgensen, W. L. Halide, Ammonium, and Alkali Metal Ion Parameters for Modeling Aqueous Solutions. *J. Chem. Theory Comput.* **2006**, *2*, 1499−1509.
(48) Lide, D. R. *Handbook of Chemistry and Physics*, 79th ed.; CRC Press: Boca Raton, FL, 1998.
(49) Alavi, S.; Ripmeester, J. A. Nonequilibrium Adiabatic Molecular Dynamics Simulations of Methane Clathrate Hydrate Decomposition. *J. Chem. Phys.* **2010**, *132*, 8.
(50) Sposito, G. Single-Particle Motions in Liquid Water. 2. The Hydrodynamic Model. *J. Chem. Phys.* **1981**, *74*, 6943−6949.
(51) Nye, P. H. Diffusion of Ions and Uncharged Solutes in Soils and Clays. *Adv. Agron.* **1979**, *31*, 225−272.
(52) Raviv, U.; Klein, J. Fluidity of Bound Hydration Layers. *Science* **2002**, *297*, 1540−1543.
(53) Raviv, U.; Laurat, P.; Klein, J. Fluidity of Water Confined to Subnanometre Films. *Nature* **2001**, *413*, 51−54.
(54) Leng, Y. S.; Cummings, P. T. Fluidity of Hydration Layers Nanoconfined between Mica Surfaces. *Phys. Rev. Lett.* **2005**, *94*, 026101.
(55) Leng, Y. S. Hydration Force and Dynamic Squeeze-out of Hydration Water under Subnanometer Confinement. *J. Phys.: Condens. Matter* **2008**, *20*, 354017.
(56) Leng, Y. S. Hydration Force between Mica Surfaces in Aqueous KCl Electrolyte Solution. *Langmuir* **2012**, *28*, 5339−5349.